



Trans. Nonferrous Met. Soc. China 25(2015) 477-482

Transactions of Nonferrous Metals Society of China

www.tnmsc.cn



Effects of Ti and Be addition on microstructure and mechanical properties of Mg_{58.5}Cu_{30.5}Y₁₁ bulk metallic glass

Ke-qiang QIU, Lin WANG, Ying-lei REN, Rong-de LI

School of Materials Science and Engineering, Shenyang University of Technology, Shenyang 110870, China Received 8 January 2014; accepted 6 April 2014

Abstract: Based on the $Mg_{58.5}Cu_{30.5}Y_{11}$ alloy, 10% Ti, 10% Be and 10% Ti, 10%

Key words: Mg-based alloy; alloying element; Ti; Be; microstructure; strength reliability

1 Introduction

Among the family of bulk metallic glasses (BMGs), glass-forming alloys are particularly interesting due to their high specific strength, abundant deposits, relatively low cost and easy recycling ability. Since Mg₆₅Cu₂₅Y₁₀ BMG [1] was firstly discovered in 1991, many valuable efforts have been devoted to researching Mg-based BMGs. In recent years, several Mg-based BMG systems with good glass forming ability (GFA) have been developed [2–7]. However, the brittle nature of almost no reliable strength for Mg-Cu-RE (RE is rare earth metal) alloys [8] makes them useless in structural application. To solve the problem of the brittleness and the strength reliability of Mg-based BMGs, alloying element addition, second phase formation and interaction with shear bands, have been proven to be the promising ways [9–11]. Therefore, many efforts [12-15] have been made, including alloying element addition or substitution with larger Poisson ratio [12,13], or with positive heat of mixing to cause phase separation [14,15] and BMG matrix composite (BMGMC) fabrication, including in-situ or ex-situ, based on Mg-based BMG.

Recently, it has been reported that the plasticity of Mg-based BMG matrix composite was improved by Ti powders dispersion [16], and the high fracture strength of $(Mg_{0.585}Cu_{0.305}Y_{0.11})_{95}Be_5$ was obtained by our group [15] due to phase-separated effect. In the present study, Mg_{58.5}Cu_{30.5}Y₁₁ alloy [3] was chosen as a basic composition because of its high glass-forming ability (GFA). While 10% Ti and 10% Be were introduced into the basic BMG to form glassy matrix composites. Meanwhile, it is noted that binary Ti-Be alloy is a glass former [17]. Therefore, the eutectic composition Ti₇₀Be₃₀ was also added into the basic alloy by up to 10% (mole fraction). In such case, we can investigate the Ti, Be and their combing effect on the microstructure as well as the corresponding mechanical properties for Mg_{58.5}Cu_{30.5}Y₁₁ alloy.

2 Experimental

The alloys with nominal compositions of $(Mg_{0.585}Cu_{0.305}Y_{0.11})_{90}X_{10}$ (X=Ti, Be) and $(Mg_{0.585}Cu_{0.305}$ -

 $Y_{0.11})_{90}(Ti_{0.7}Be_{0.3})_{10}$ (mole fraction, %) were investigated in this study. The intermediate alloys containing Cu, Y, Ti and/or Be (99.9% or higher, mass fraction) were prepared by arc melting under a Ti-gettered argon atmosphere in a water-cooled copper crucible. The ingots were melted several times to ensure their chemical homogeneity. The master alloys were melted with Mg (99.95%, mass fraction) by induction melting method under argon atmosphere. The alloys were then broken into pieces and re-melted again in the same furnace by using quartz tubes as crucibles. The as-cast cylindrical samples with 3 mm in diameter for the designed alloys were obtained by injecting the melting liquid into the cavity of copper corresponding mould. cross-sectional surfaces of the as-cast samples were analyzed by X-ray diffraction (XRD) (Rigaku D/max 2400). The thermal stability of the alloys was investigated by differential scanning calorimeter (DSC) (Q100 V9.0 Build 275) at a heating rate of 20 K/min. The microstructures and the fracture surfaces of the as-cast samples were examined by scanning electron microscope (SEM, S3400N) linked with an energy dispersive spectrometer (EDS). The specimens with an aspect ratio of 2:1 (ratio of height to diameter) were tested by uniaxial compression with an initial strain rate of $1 \times 10^{-4} \text{ s}^{-1}$ at room temperature using an Instron-type (Model 55100) machine. The loading surfaces of the specimens were polished to be parallel to each other to ensure the uniaxial loading. At least ten samples of each alloy were tested considering the strength dispersive nature and reliability. Nanoindentation test was performed for the $(Mg_{0.585}Cu_{0.305}Y_{0.11})_{90}(Ti_{0.7}Be_{0.3})_{10}$ alloy by MTS-nanoindenter. Prior to indentation, the samples were cut into disks of approximately 1 mm in thickness and carefully polished.

3 Results and discussion

Figure 1 shows the XRD patterns taken from the transverse cross section of the as-cast (Mg_{0.585}Cu_{0.305}- $Y_{0.11})_{90}X_{10}$ (X=Ti, Be), $(Mg_{0.585}Cu_{0.305}Y_{0.11})_{90}(Ti_{0.7}Be_{0.3})_{10}$ and Mg_{58.5}Cu_{30.5}Y₁₁ alloys with 3 mm in diameter. Different from $Mg_{58.5}Cu_{30.5}Y_{11}$ BMG, the sharp diffraction peaks corresponding to the crystalline phases in addition to the broad diffraction peaks for the three designed alloys are observed, indicating the coexistence of the crystalline and the amorphous phases. The crystalline phases were identified as CuY phase for $(Mg_{0.585}Cu_{0.305}Y_{0.11})_{90}Be_{10}$ alloy and CuTi phase for $(Mg_{0.585}Cu_{0.305}Y_{0.11})_{90}Ti_{10}$ and $(Mg_{0.585}Cu_{0.305}Y_{0.11})_{90}$ (Ti_{0.7}Be_{0.3})₁₀ alloys. While there are some deviations of the position of peaks for the $(Mg_{0.585}Cu_{0.305}Y_{0.11})_{90}Be_{10}$ and $(Mg_{0.585}Cu_{0.305}Y_{0.11})_{90}(Ti_{0.7}Be_{0.3})_{10}$ alloys due to the solution difference of Be element. It is worth pointing out that the phase is too ambiguous to be completely confirmed from XRD curve for $(Mg_{0.585}Cu_{0.305}Y_{0.11})_{90}$ -Be₁₀ alloy due to the relatively low intensity of the sharp diffraction peak, which will be further confirmed in the following section.

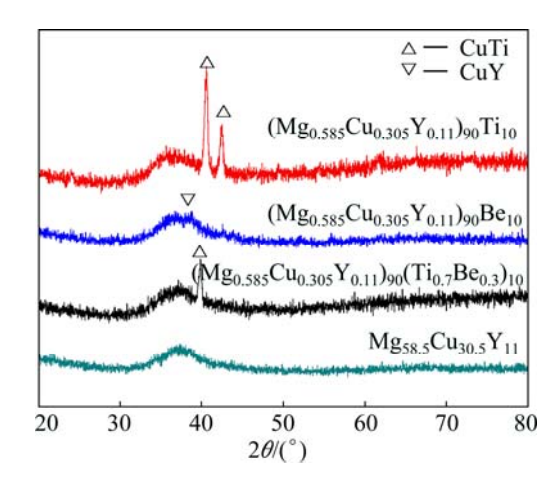
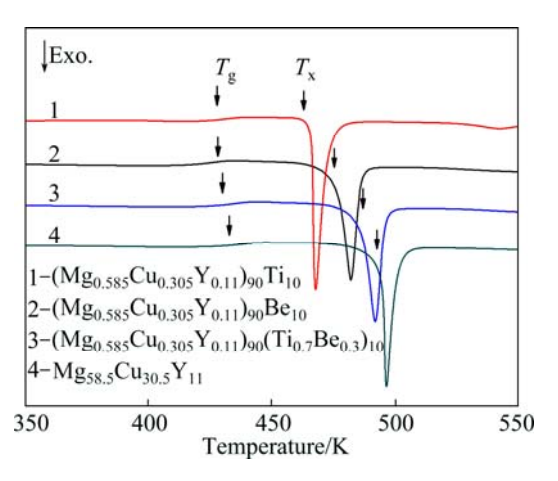


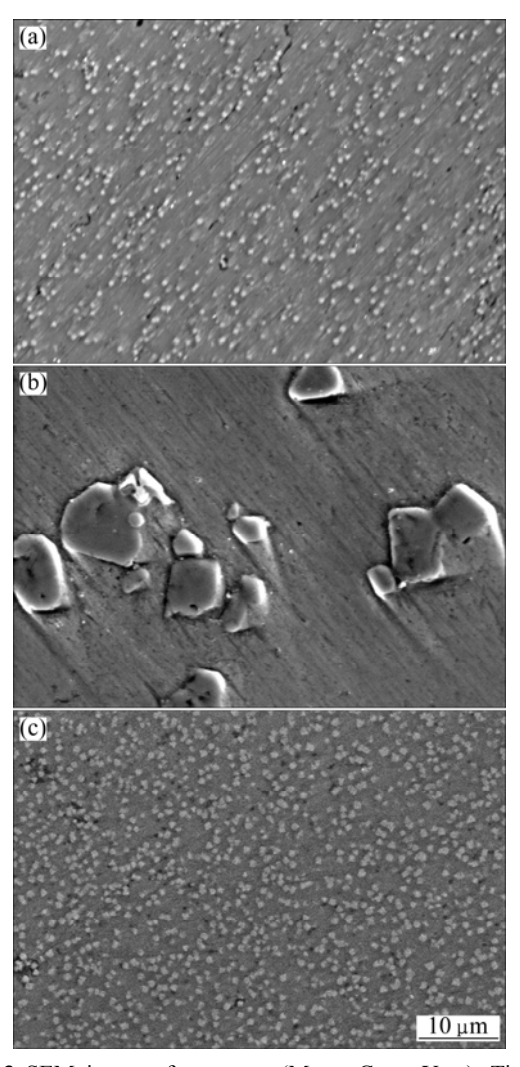
Fig. 1 XRD patterns for as-cast $(Mg_{0.585}Cu_{0.305}Y_{0.11})_{90}X_{10}$ (X=Ti, Be), $(Mg_{0.585}Cu_{0.305}Y_{0.11})_{90}(Ti_{0.7}Be_{0.3})_{10}$ and $Mg_{58.5}-Cu_{30.5}Y_{11}$ alloys with 3 mm in diameter

The DSC curves for the as-cast (Mg_{0.585}Cu_{0.305}- $Y_{0.11})_{90}X_{10}$ (X=Ti, Be) and $(Mg_{0.585}Cu_{0.305}Y_{0.11})_{90}$ -(Ti_{0.7}Be_{0.3})₁₀ alloys obtained at a heating rate of 20 K/min are shown in Fig. 2. The curve of Mg_{58.5}Cu_{30.5}Y₁₁ is also presented for comparison. Obvious glass transition followed by a supercooled liquid region and exothermic reaction corresponding to the crystallization for the alloys are observed. The glass-transition temperatures $(T_{\rm g})$ of the four alloys are almost the same, but the supercooled liquid regions (ΔT_x) decrease from 67 K for $Mg_{58.5}Cu_{30.5}Y_{11}$ to 37. 48 and 58 K $(Mg_{0.585}Cu_{0.305}Y_{0.11})_{90}Ti_{10}$, $(Mg_{0.585}Cu_{0.305}Y_{0.11})_{90}Be_{10}$ and $(Mg_{0.585}Cu_{0.305}Y_{0.11})_{90}(Ti_{0.7}Be_{0.3})_{10}$ alloys, respectively. The reason for this phenomenon is that the $T_{\rm g}$ value is



related to glassy matrix formation, whereas ΔT_x is influenced by the formation of crystalline phases. The DSC results indicate that the supercooled liquid region of the designed alloys decreases due to the addition of alloying elements Ti and Be.

In order to clarify the distribution, morphology and composition of the crystalline phases in the glassy matrix, SEM and EDS were employed to analyze the microstructures of the cross section of the as-cast samples. The microstructures of the alloys shown in Fig. 3 were taken from the center of the samples. From Fig. 3(a), a great number of white particles corresponding to CuTi intermetallic phase for (Mg_{0.585}Cu_{0.305}Y_{0.11})₉₀Ti₁₀ alloy are observed. It is shown that the particles are very tiny (with the diameter less than 0.5 μm) and dispersed uniformly in the glassy matrix. In Fig. 3(b), for (Mg_{0.585}Cu_{0.305}Y_{0.11})₉₀Be₁₀ alloy, some second phases with polygon shape and sizes not larger than 10 μm for the side length are heterogeneously distributed in the glassy matrix. The EDS results for the



 $\begin{array}{llll} \textbf{Fig. 3} & SEM & images & for as-cast & (Mg_{0.585}Cu_{0.305}Y_{0.11})_{90}Ti_{10} & (a), \\ (Mg_{0.585}Cu_{0.305}Y_{0.11})_{90}Be_{10} & (b) & and & (Mg_{0.585}Cu_{0.305}Y_{0.11})_{90}-(Ti_{0.7}Be_{0.3})_{10} & (c) & alloys & with 3 & mm & in diameter \\ \end{array}$

second phase give a composition of Cu_{56.65}Y_{43.35}, the composition of glass matrix is Mg_{64.2}Cu_{26.59}Y_{9.21} (element Be cannot be indicated from the EDS analysis). The composition and morphology of the second phase are similar to those of the $(Mg_{0.585}Cu_{0.305}Y_{0.11})_{95}Be_5$ alloy [15]. It is suggested that there is no much difference in the phase change with the increase of Be content due to its infinite solubility in the magnesium. Therefore, the second phase is also the CuYBe glassy phase containing CuY crystals formed by phase-separated reaction as the evidence given by our previous investigation [15]. Figure 3(c) shows the microstructure of $(Mg_{0.585}Cu_{0.305}Y_{0.11})_{90}(Ti_{0.7}Be_{0.3})_{10}$, which presents an almost the same morphology as Fig. 3(a). Compared with the second phase in (Mg_{0.585}Cu_{0.305}- $Y_{0.11})_{90}Ti_{10}$, however, the number and the size of the particles in $(Mg_{0.585}Cu_{0.305}Y_{0.11})_{90}(Ti_{0.7}Be_{0.3})_{10}$ are more and much larger. From the EDS measurements, we can estimate that the average compositions of the particles the matrix are $Mg_{3.91}Cu_{48.72}Y_{2.26}Ti_{45.11}$, and $Mg_{63.38}Cu_{23.36}Y_{10.94}Ti_{2.32}$ for $(Mg_{0.585}Cu_{0.305}Y_{0.11})_{90}Ti_{10}$ and $Mg_{2.96}Cu_{47.39}Y_{3.43}Ti_{46.22}$, $Mg_{65.58}Cu_{22.25}Y_{9.52}Ti_{2.65}$ for $(Mg_{0.585}Cu_{0.305}Y_{0.11})_{90}(Ti_{0.7}Be_{0.3})_{10},$ respectively. $(Mg_{0.585}Cu_{0.305}Y_{0.11})_{90}(Ti_{0.7}Be_{0.3})_{10}$, it is suggested that element Be is mainly distributed in the CuTi particles due to the better combining capacity among Cu, Ti and Be. Considering the particle number and size vs the XRD intensity shown in Fig. 1, it is possible for some of the particles containing glassy phases on account of the excellent GFA of ternary and/or quaternary glass former systems containing Cu, Ti and/or Be [17,18]. That is why the intensity of the sharp diffraction peak in XRD curve for $(Mg_{0.585}Cu_{0.305}Y_{0.11})_{90}(Ti_{0.7}Be_{0.3})_{10}$ is lower than that of $(Mg_{0.585}Cu_{0.305}Y_{0.11})_{90}Ti_{10}$.

Compressive tests were performed to investigate the effects of crystalline phases on mechanical properties of the alloys. Figure 4 shows the stress-strain curves of the alloys with the largest fracture strength among 10 samples for each alloy. The largest fracture strengths for $(Mg_{0.585}Cu_{0.305}Y_{0.11})_{90}Ti_{10}$, $(Mg_{0.585}Cu_{0.305}Y_{0.11})_{90}Be_{10}$ and $(Mg_{0.585}Cu_{0.305}Y_{0.11})_{90}(Ti_{0.7}Be_{0.3})_{10}$ alloys are 797.6, 952.6 and 1007.8 MPa, respectively. Compared with Mg_{58.5}Cu_{30.5}Y₁₁ BMG (681 MPa), the strengths of the designed alloys are obviously increased by about 17%, 40% and 48%, respectively. We notice that there are about 5.1%, 3.9%, 4.8% and 15.5% difference between the smallest and the largest fracture strengths for $(Mg_{0.585}Cu_{0.305}Y_{0.11})_{90}Ti_{10},$ $(Mg_{0.585}Cu_{0.305}Y_{0.11})_{90}Be_{10},$ $(Mg_{0.585}Cu_{0.305}Y_{0.11})_{90}(Ti_{0.7}Be_{0.3})_{10}$ and $Mg_{58.5}Cu_{30.5}Y_{11}$, respectively. According to the fracture strength distribution region or Weibull modulus analysis [19], we conclude that the strength reliability for Mg_{58.5}Cu_{30.5}Y₁₁ is in trusted range by addition of 10% Ti, 10% Be and 10% Ti₇₀Be₃₀ (mole fraction), whereas the strength for

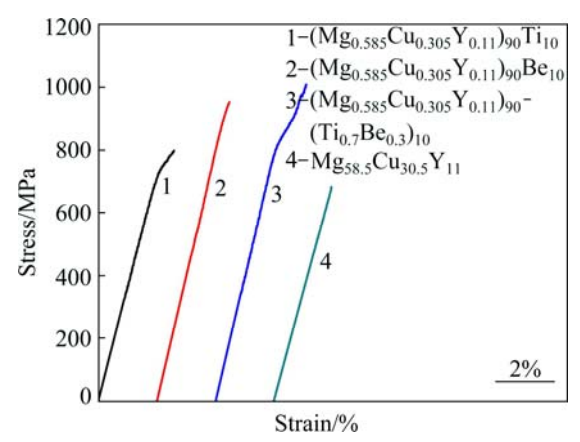


Fig. 4 Compressive stress—strain curves of as-cast $(Mg_{0.585}Cu_{0.305}Y_{0.11})_{90}X_{10}$ (X=Ti, Be), $(Mg_{0.585}Cu_{0.305}Y_{0.11})_{90}$ - $(Ti_{0.7}Be_{0.3})_{10}$ and $Mg_{58.5}Cu_{30.5}Y_{11}$ alloys with 3 mm in diameter

Mg_{58.5}Cu_{30.5}Y₁₁ itself cannot be trusted due to high level up to 10% fracture strength difference for different samples. Furthermore, the degree of the reliability from high to low level is in the order of Be, Ti-Be and Ti addition, which is also an unexpected result by considering the microstructure shown in Fig. 3. The even distribution of the second phase in Figs. 3(a) and (c) is generally believed that the alloys present better mechanical properties than the uneven one as shown in Fig. 3(d). However, they did not present much better properties than what expected. But some differences can be found from the slope of the end part of the stress-strain curves even for the two alloys with similar microstructures. The slope change and strength increase are typical phenomena of yielding of glassy matrix and the hardening of CuTi phase during compressive process. Therefore, the CuTi phase can not only act as barriers for shear band propagation, but also present a hardening effect. The hardness values measured by nanoindentation for the Mg-rich matrix and the CuTi phase in $(Mg_{0.585}Cu_{0.305}Y_{0.11})_{90}(Ti_{0.7}Be_{0.3})_{10}$ glassy composite are (2.2 ± 0.05) and (4.1 ± 0.05) GPa, respectively, indicating the harder nature of the latter. It should be noticed that the hardening effect for the second phase is rarely observed because the second phase is either too hard or too soft. The hardening ability can only come from the phase that can deform and yield at almost the same yield strength level as the matrix alloy, which is corresponding to the strength of CuTi interstitial solid intermetallic compound.

Figure 5 presents the fracture surfaces of the three investigated alloys. For 10% Ti-containing alloy shown in Fig. 5(a), well-developed vein patterns are observed, suggesting the local softening or melting inside the shear bands [20]. Meanwhile, CuTi particles distributed on the fracture surface are obviously observed. For 10% Be-containing alloy shown in Fig. 5(b), the traces of the

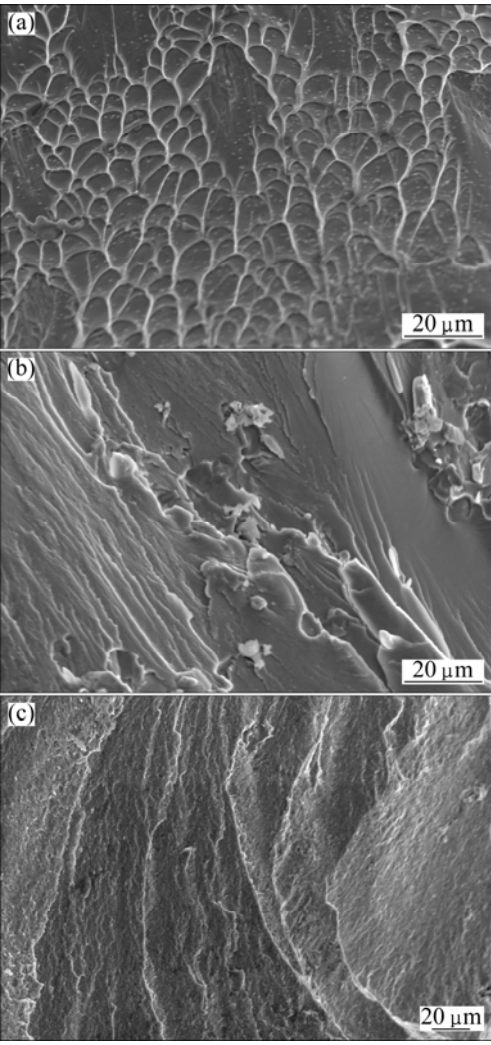


Fig. 5 SEM images of fracture surfaces for as-cast $(Mg_{0.585}Cu_{0.305}Y_{0.11})_{90}Ti_{10}$ (a), $(Mg_{0.585}Cu_{0.305}Y_{0.11})_{90}Be_{10}$ (b) and $(Mg_{0.585}Cu_{0.305}Y_{0.11})_{90}(Ti_{0.7}Be_{0.3})_{10}$ (c) alloys

second phase departure without any crack suggest that the second phase can increase the toughness of the composite. While for the Ti₇₀Be₃₀-containing alloy shown in Fig. 5(c), the fluctuant fractured surface with many large steps indicating multiple shear processes are in action during the fracture. While many ripples on step surfaces seem to come from the tiny-white particles in the matrix. These kinds of fracture surfaces indicate that the toughness of the designed alloys is improved, which is consistent with their higher fracture strength. However, the alloys with the similar microstructure and phase constituent (shown in Figs. 3(a) and (c), respectively) present totally different fracture surfaces (shown in Figs. 5(a) and (c), respectively), which may be related to stress condition for different alloys. For Ti-containing alloy, only single shear stress is across the fracture surface, therefore, very smooth surface with vein patterns that come from the softening effect during fracturing process and the white particles present no obvious effect on the

last stage of departure parts. For the Ti₇₀Be₃₀-containing alloy, multiple shear bands act and interfere with each other, and the white particles present obvious effect even on the last stage of departure parts. While for the Be-containing alloy, the in-situ second glassy phase is so large that it cannot induce many shear bands to obviously show the yielding of the matrix material. Therefore, the strength of the Be-containing alloy is controlled by the matrix. From this point of view, the yielding processes of other two alloys, by contrary, are controlled by the tiny second phases due to shear band interaction.

4 Conclusions

- 1) The CuTi phase is distributed in $(Mg_{0.585}Cu_{0.305}Y_{0.11})_{90}Ti_{10}$ and $(Mg_{0.585}Cu_{0.305}Y_{0.11})_{90}-(Ti_{0.7}Be_{0.3})_{10}$ alloys, while the CuYBe glassy phase containing CuY crystals is embedded in the matrix of $(Mg_{0.585}Cu_{0.305}Y_{0.11})_{90}Be_{10}$ alloy.
- 2) The largest fracture strengths of the samples with 3 mm in diameter for $(Mg_{0.585}Cu_{0.305}Y_{0.11})_{90}Ti_{10}$, $(Mg_{0.585}Cu_{0.305}Y_{0.11})_{90}Be_{10}$ and $(Mg_{0.585}Cu_{0.305}Y_{0.11})_{90}-(Ti_{0.7}Be_{0.3})_{10}$ alloys are 797.6, 952.6 and 1007.8 MPa, respectively. Compared with $Mg_{58.5}Cu_{30.5}Y_{11}$ BMG, the strengths of the designed alloys are increased by about 17%, 40% and 48%, respectively.
- 3) Compared with difference (15.5%) between the smallest and the largest fracture strength for Mg_{58.5}Cu_{30.5}Y₁₁, those of 5.1%, 3.9% and 4.8% for the (Mg_{0.585}Cu_{0.305}Y_{0.11})₉₀Ti₁₀, (Mg_{0.585}Cu_{0.305}Y_{0.11})₉₀Be₁₀ and (Mg_{0.585}Cu_{0.305}Y_{0.11})₉₀(Ti_{0.7}Be_{0.3})₁₀ alloys were obtained, respectively, indicating that their strength reliabilities are greatly improved by alloying element addition.
- 4) The tiny second phases existing in the $(Mg_{0.585}Cu_{0.305}Y_{0.11})_{90}Ti_{10}$ and $(Mg_{0.585}Cu_{0.305}Y_{0.11})_{90}-(Ti_{0.7}Be_{0.3})_{10}$ glassy matrix composites can induce yielding of the matrix material, while larger second glassy phase existing in $(Mg_{0.585}Cu_{0.305}Y_{0.11})_{90}Be_{10}$ glassy matrix does not present such effect.

References

- INOUE A, NAKAMURA T, NISHIYAMA N, MASUMOTO T. Mg-Cu-Y bulk amorphous alloys with high tensile strength produced by a high-pressure die casting method [J]. Materials Transactions, JIM, 1992, 33(10): 937–945.
- [2] INOUE A, KATO A, ZHANG T. Mg-Cu-Y amorphous alloys with high mechanical strengths produced by a metallic mold casting method [J]. Materials Transactions, JIM, 1991, 32(7): 609-616.
- [3] MA H, ZHENG Q, XU J, LI Y, MA E. Doubling the critical size for bulk metallic glass formation in the Mg-Cu-Y ternary system [J]. Journal of Materials Research, 2005, 20(9): 2252–2255.
- [4] XI X K, WANG R J, ZHAO D Q, PAN M X, WANG W H.

- Glass-forming Mg–Cu–RE (RE=Gd, Pr, Nd, Tb, Y, and Dy) alloys with strong oxygen resistance in manufacturability [J]. Journal of Non-Crystalline Solids, 2004, 344(3): 105–109.
- [5] YUAN G Y, INOUE A. The effect of Ni substitution on the glass-forming ability and mechanical properties of Mg-Cu-Gd metallic glass alloys [J]. Journal of Alloys and Compounds, 2005, 387(1-2): 134-138.
- [6] MA H, MA E, XU J. A new Mg₆₅Cu_{7.5}Ni_{7.5}Zn₅Ag₅Y₁₀ bulk metallic glass with strong glass-forming ability [J]. Journal of Materials Research, 2003, 18(10): 2288–2291.
- [7] PARK E S, CHANG H J, KIM D H. Mg-rich Mg-Ni-Gd ternary bulk metallic glasses with high compressive specific strength and ductility [J]. Journal of Materials Research, 2007, 22(2): 334–338.
- [8] LI Q F, QIU K Q, YANG X, YUAN X G, ZHANG T. Glass forming ability and reliability in fracture stress for Mg-Cu-Ni-Nd-Y bulk metallic glasses [J]. Materials Science and Engineering A, 2008, 491(1-2): 420-424.
- [9] DAS J, TANG M B, KIM K B, THEISSMANN R, BAIER F, WANG W H, ECKERT J. "Work-hardenable" ductile bulk metallic glass [J]. Physical Review Letters, 2005, 94(20): 205501.
- [10] HOFMANN D C, SUH J Y, WIEST A, DUAN G, LIND M L, DEMETRIOU M D, JOHNSON W L. Designing metallic glass matrix composites with high toughness and tensile ductility [J]. Nature, 2008, 451(28): 1085–1089.
- [11] BROTHERS A H, DUNAND D C, ZHENG Q, XU J. Amorphous Mg-based metal foams with ductile hollow spheres [J]. Journal of Applied Physics, 2007, 102(2): 023508.
- [12] PAN D G, LIU W Y, ZHANG H F, WANG A M, HU Z Q. Mg-Cu-Ag-Gd-Ni bulk metallic glass with high mechanical strength [J]. Journal of Alloys and Compounds, 2007, 438(1-2): 142-144.
- [13] ZHENG Q, MA H, MA E, XU J. Mg-Cu-(Y,Nd) pseudo-ternary bulk metallic glasses: The effects of Nd on glass-forming ability and plasticity [J]. Scripta Materialia, 2006, 55(6): 541–544.
- [14] REN Y L, ZHU R L, SUN J, YOU J H, QIU K Q. Phase separation and plastic deformation in an Mg-based bulk metallic glass [J]. Journal of Alloys and Compounds, 2010, 493(1): L42–L46.
- [15] WANG L, QIU K Q, YOU J H, REN Y L, LI R D. Phase separation and sample size independence of fracture strength for (Mg_{0.585}Cu_{0.305}Y_{0.11})₉₅Be₅ bulk metallic glass [J]. Journal of Non-Crystalline Solids, 2013, 370: 1–5.
- [16] KINAKA M, KATO H, HASEGAWA M, INOUE A. High specific strength Mg-based bulk metallic glass matrix composite highly ductilized by Ti dispersoid [J]. Materials Science and Engineering A, 2008, 494(1-2): 299-30.
- [17] TANNER L E, RAY R. Metallic glass formation and properties in Zr and Ti alloyed with Be in the binary Zr–Be and Ti–Be systems [J]. Acta Metallurgica, 1979, 27(11): 1727–1747.
- [18] WIEST A, DUAN G, DEMETRIOU M D, WIEST L A, PECK A, KALTENBOECK G, WIEST B, JOHNSON W L. Zr-Ti-based Be-bearing glasses optimized for high thermal stability and thermoplastic formability [J]. Acta Materialia, 2008, 56(11): 2625-2630.
- [19] KHALILI A, KROMP K. Statistical properties of Weibull estimators [J]. Journal of Materials Science, 1991, 26(24): 6741–6752.
- [20] WRIGHT W J, SAHA R, NIX W D. Deformation mechanisms of the $Zr_{40}Ti_{14}Ni_{10}Cu_{12}Be_{24} \ bulk \ metallic \ glass \ [J]. \ Materials \ Transactions, \\ JIM, 2001, 42(4): 642–649.$

$Ti \ n \ Be \ y \ Mg_{58.5}Cu_{30.5}Y_{11}$ 大块金属玻璃显微组织和力学性能的影响

邱克强, 王 琳, 任英磊, 李荣德

沈阳工业大学 材料科学与工程学院, 沈阳 110870

摘 要: 以 $Mg_{58.5}Cu_{30.5}Y_{11}$ 合金为基础分别加入含量为 10%(摩尔分数)的 Ti、Be 和 $Ti_{70}Be_{30}$,通过传统铜模铸造法制备直径为 3 mm 的试样。分别采用 X 射线衍射仪、差示扫描量热计和扫描电子显微镜研究合金的相组成、热稳定性和显微组织。讨论合金元素 Ti 和 Be 对 $Mg_{58.5}Cu_{30.5}Y_{11}$ 块体金属玻璃的显微组织和力学性能的影响。结果表明, $(Mg_{0.585}Cu_{0.305}Y_{0.11})_{90}Ti_{10}$ 和 $(Mg_{0.585}Cu_{0.305}Y_{0.11})_{90}(Ti_{0.7}Be_{0.3})_{10}$ 合金中分布着 CuTi 相,而 $(Mg_{0.585}Cu_{0.305}Y_{0.11})_{90}-Be_{10}$ 合金基体中镶嵌着含有 CuY 晶体的 CuYBe 非晶相。在单轴压缩载荷下, $(Mg_{0.585}Cu_{0.305}Y_{0.11})_{90}Ti_{10}$ 、 $(Mg_{0.585}Cu_{0.305}Y_{0.11})_{90}Be_{10}$ 和 $(Mg_{0.585}Cu_{0.305}Y_{0.11})_{90}(Ti_{0.7}Be_{0.3})_{10}$ 合金的最大压缩断裂强度分别为 797.6、952.6 和 1007.8 MPa,比 $Mg_{58.5}Cu_{30.5}Y_{11}$ 合金的强度分别提高了 17%、40%和 48%。根据每种合金 10 个试样的强度分布范围推断这 3 种合金的强度可靠性得到了很大提高。

关键词: Mg 基合金; 合金元素; Ti; Be; 显微组织; 强度可靠性

(Edited by Wei-ping CHEN)